

Inverse obstacle scattering in two dimensions with multiple frequency data and multiple angles of incidence

Carlos Borges¹ and Leslie Greengard^{1,2}

¹Courant Institute of Mathematical Sciences, New York University

²Simons Center for Data Analysis, Simons Foundation, New York, NY

Received: date / Accepted: date

Abstract

We consider the problem of reconstructing the shape of an impenetrable sound-soft obstacle from scattering measurements. The input data is assumed to be the far-field pattern generated when a plane wave impinges on an unknown obstacle from one or more directions and at one or more frequencies. It is well known that this inverse scattering problem is both ill posed and nonlinear. It is common practice to overcome the ill posedness through the use of a penalty method or Tikhonov regularization. Here, we present a more physical regularization, based simply on restricting the unknown boundary to be band-limited in a suitable sense. To overcome the nonlinearity of the problem, we use a variant of Newton's method. When multiple frequency data is available, we supplement Newton's method with the recursive linearization approach due to Chen.

During the course of solving the inverse problem, we need to compute the solution to a large number of forward scattering problems. For this, we use high-order accurate integral equation discretizations, coupled with fast direct solvers when the problem is sufficiently large.

1 Introduction

Inverse problems arise in many parts of science and engineering, including medical imaging, remote sensing, ocean acoustics, nondestructive testing, geophysics and radar [1, 2, 3, 4]. In this paper, we concentrate on the problem of recovering the shape of an unknown obstacle embedded in a homogeneous medium from far-field acoustic scattering measurements in two space dimensions. We assume that the object Ω is impenetrable and “sound-soft” with boundary Γ . We restrict our attention here to the time harmonic setting, in which case the governing equation is the Helmholtz equation

$$\Delta u(\mathbf{x}) + k^2 u(\mathbf{x}) = 0, \quad \mathbf{x} \in \mathbb{R}^2 \setminus \overline{\Omega}.$$

In the sound-soft case, u must satisfy the Dirichlet condition

$$u(\mathbf{x}) = 0, \quad \text{for } \mathbf{x} \in \Gamma.$$

Following standard practice, we write

$$u(\mathbf{x}) = u^{\text{inc}}(\mathbf{x}) + u^{\text{scat}}(\mathbf{x}),$$

where u^{inc} denotes a known incoming field and u^{scat} denotes the scattered field. We will assume that the incoming field is a plane wave $u^{\text{inc}}(\mathbf{x}) = \exp(ik\mathbf{x} \cdot \mathbf{d})$, where \mathbf{d} is a unit vector that defines the direction of propagation.

It is well-known that radiating fields have a simple asymptotic structure as $|\mathbf{x}| \rightarrow \infty$. More precisely [1],

Lemma 1.1 *Let (r, θ) denote the polar coordinates of the point \mathbf{x} . Every radiating solution u^{scat} to the Helmholtz equation has the asymptotic behavior of an outgoing cylindrical wave:*

$$u^{\text{scat}}(\mathbf{x}) = \frac{e^{ikr}}{r^{1/2}} \left\{ u^\infty(\theta) + \mathcal{O}\left(\frac{1}{r^{3/2}}\right) \right\}, \quad r \rightarrow \infty,$$

uniformly in all directions θ . The function u^∞ is defined on the unit circle U and referred to as the far-field pattern of u^{scat} .

Definition 1.1 *Suppose that u^{inc} and the domain shape Γ are known. The forward scattering problem consists of solving the boundary value problem:*

$$\Delta u^{\text{scat}}(\mathbf{x}) + k^2 u^{\text{scat}}(\mathbf{x}) = 0 \quad \text{in } \mathbb{R}^2 \setminus \overline{\Omega} \quad (1)$$

$$u^{\text{scat}}(\mathbf{x}) = -u^{\text{inc}}(\mathbf{x}) \quad \text{in } \Gamma, \quad (2)$$

where $u^{\text{scat}} \in C^2(\mathbb{R}^2 \setminus \overline{\Omega}) \cap C(\mathbb{R}^2 \setminus \Omega)$. The scattered field must satisfy the Sommerfeld radiation condition

$$\lim_{r \rightarrow \infty} r^{1/2} \left(\frac{\partial u^{\text{scat}}}{\partial r} - iku^{\text{scat}} \right) = 0, \quad r = |\mathbf{x}|.$$

We show in the next section how to compute $u^\infty(\theta)$ from an integral representation for u^{scat} . For the moment, we simply denote this mapping, from the curve to the far-field pattern as

$$F(\Gamma) = u^\infty. \quad (3)$$

Definition 1.2 *The inverse scattering problem consists of determining Γ from $u^\infty(\theta)$. This requires solving the nonlinear functional equation (3).*

The forward problem is both linear and well-posed, although it does require the solution of a partial differential equation. The inverse problem, however, is quite different. It is both nonlinear and ill-posed, so that the development of robust and stable solvers remains quite challenging. The nonlinearity leads to a non-convex optimization problem and the ill-posedness requires some form of regularization. For discussion of the question of uniqueness, we refer the reader to [1, 5].

Following [5], we note that several approaches have been developed to handle the nonlinearity. They can be classified as iterative methods, decomposition methods, and sampling methods. The iterative category includes Newton's method, Landweber iteration and the nonlinear conjugate gradient method [1, 6, 7]. Decomposition methods proceed by first finding an equivalent source representation that leads to the measured far-field pattern with sources located inside Ω . (The suitable placement of sources requires some prior knowledge about the scatterer.) Once this linear

(but ill-posed) problem has been solved, it remains to solve the well-posed, but nonlinear, problem of determining Γ , using the fact that the total field $u^{\text{inc}} + u^{\text{scat}}$ vanishes there [8, 9, 10, 11]. Finally, in sampling methods, one seeks to compute an “indicator” function which vanishes inside Ω . This category includes the linear sampling method of Colton and Kirsch [12], the singular source method of Potthast [13, 11], the factorization method of Kirsch [14], and the probe method of Ikehata [15]. We refer the interested reader to the tutorial article [5] and the text [1] for further background material. The ill-posedness of the inverse problem is usually addressed by using some variant of Tikhonov regularization for the linearized problems which arise in each of the schemes listed above [16, 1, 17, 3].

In this paper, we present a Newton-like iterative method for the inverse obstacle scattering problem with several new features. First, unlike many obstacle scattering algorithms, we do *not* assume the boundary is star-shaped. Instead, we assume it is bandlimited as a function of arclength but otherwise unconstrained. Second, instead of Tikhonov regularization, we simply enforce a band-limit on the reconstructed curve using the method of [18]. Third, we make use of efficient, high-order forward modeling capabilities. After describing the single frequency reconstruction problem, we investigate the quality of reconstruction using multiple angles of incidence as well as multiple frequencies. In the latter case, we rely on the recursive linearization approach developed by Chen [19], and employed previously by Sini and Thành [20] for impenetrable sound-soft obstacles (the same problem considered here). Recursive linearization was also studied by Bao and Triki [21] for the solution of the inverse medium problem.

In Section 2, we briefly review the direct scattering problem and its solution using integral equation methods. In Section 3.1, we describe the inverse scattering problem in more detail for a single frequency, its linearization and its solution using a Newton-like method. We also describe our regularization based on band-limited approximation. In section 3.2, we consider multiple frequency data and the recursive linearization approach. In Section 5, we illustrate the performance of our method, while section 6 contains some concluding remarks and a brief discussion of future directions for research.

2 The direct scattering problem

In this section, we briefly review the solution of the forward acoustic scattering problem for sound-soft impenetrable objects in two dimensions. We refer the reader to [1] for a proof of uniqueness. We simply note here that, in addition to being unique, the solution depends continuously on the data u^{inc} in the maximum norm.

We will make use of a boundary integral approach, since this requires discretization of Γ alone and permits the imposition of the exact Sommerfeld radiation condition. We refer the interested reader to [1, 22] for a review of the relevant potential theory.

Definition 2.1 *Given a boundary Γ in \mathbb{R}^2 , the single layer potential is defined by*

$$[S_{\Gamma,k}\varphi](\mathbf{x}) := \int_{\Gamma} G_k(\mathbf{x}, \mathbf{y}) \varphi(\mathbf{y}) \, ds(\mathbf{y}),$$

and the double layer potential is defined by

$$[D_{\Gamma,k}\varphi](\mathbf{x}) := \int_{\Gamma} \frac{\partial G_k(\mathbf{x}, \mathbf{y})}{\partial \nu(\mathbf{y})} \varphi(\mathbf{y}) \, ds(\mathbf{y}).$$

The normal derivative of the single layer operator is defined by

$$[S'_{\Gamma,k}\varphi](\mathbf{x}) := \int_{\Gamma} \frac{\partial G_k(\mathbf{x}, \mathbf{y})}{\partial \nu(\mathbf{x})} \varphi(\mathbf{y}) \, ds(\mathbf{y}).$$

Here, $G_k(r) = \frac{i}{4}H_0(kr)$ is the Green's function for the Helmholtz equation that satisfies the outgoing radiation condition, where H_0 denotes the Hankel function of the first kind. We note that $S_{\Gamma,k}$ is weakly singular and the integral is well-defined for any \mathbf{x} . The limiting value of $D_{\Gamma,k}$ depends on the side of Γ from which \mathbf{x} approaches the curve. For $\mathbf{x} \in \Gamma$, $D_{\Gamma,k}$ is defined in the principal value sense. Note that $S'_{\Gamma,k}$ is the adjoint of $D_{\Gamma,k}$ and should also be interpreted in a principal value sense when $\mathbf{x} \in \Gamma$.

Remark 2.1 When the frequency k under consideration is clear from context, we will write $S_{\Gamma}, D_{\Gamma}, S'_{\Gamma}$ instead of $S_{\Gamma,k}, D_{\Gamma,k}, S'_{\Gamma,k}$.

Using the asymptotic behavior of the Hankel function as $r \rightarrow \infty$, we have simple formulas for the far-field patterns of the single and double layer potentials [1]. The far-field pattern of the single layer potential is given by

$$[S_{\Gamma,k}^{\infty}\varphi](\theta) := \frac{e^{i\pi/4}}{\sqrt{8\pi k}} \int_{\Gamma} e^{-ik(\cos\theta, \sin\theta) \cdot \mathbf{y}} \varphi(\mathbf{y}) \, ds(\mathbf{y}), \quad \theta \in U. \quad (4)$$

U here is the unit circle. The far-field pattern of the double layer potential is given by

$$[D_{\Gamma,k}^{\infty}\varphi](\theta) := e^{-i\pi/4} \sqrt{\frac{k}{8\pi}} \int_{\Gamma} e^{-ik(\cos\theta, \sin\theta) \cdot \mathbf{y}} ((\cos\theta, \sin\theta) \cdot \nu(\mathbf{y})) \varphi(\mathbf{y}) \, ds(\mathbf{y}). \quad (5)$$

2.1 The combined field integral equation

Two distinct methods for solving the forward scattering problem will be needed in our inverse scattering algorithm. The first is based on representing the scattered field as a linear combination of single and double layer potentials with the same density:

$$u^{\text{scat}}(x) := [D_{\Gamma,k}\varphi](\mathbf{x}) - i\eta [S_{\Gamma,k}\varphi](\mathbf{x}), \quad \mathbf{x} \in \mathbb{R}^2 \setminus \overline{\Omega},$$

where η is a coupling parameter chosen to be proportional to the frequency of the incident wave [23]. Imposing the boundary condition (2) and using standard jump relations for the double layer potential [1, 22], we obtain for $\mathbf{x} \in \Gamma$, the integral equation

$$\left[\left(\frac{1}{2}I + D_{\Gamma,k} - i\eta S_{\Gamma,k} \right) \varphi \right](\mathbf{x}) = -u^{\text{inc}}(\mathbf{x}), \quad (6)$$

where I is the identity operator. This is a well-conditioned, resonance free Fredholm equation of the second kind [1].

Once φ is known, we may easily compute the far-field pattern $u^{\infty}(\theta)$ by using (4) and (5):

$$u^{\infty}(\theta) = [(D_{\Gamma,k}^{\infty} - i\eta S_{\Gamma,k}^{\infty})\varphi](\theta). \quad (7)$$

2.2 Green's representation

A second method for solving the forward problem can be obtained by applying Green's second identity to u^{scat} and u^{inc} separately, together with the boundary condition (2). A straightforward calculation shows that

$$u(\mathbf{x}) = u^{\text{inc}}(\mathbf{x}) - \left[S_{\Gamma,k} \frac{\partial u}{\partial \nu} \right](\mathbf{x}), \quad x \in \mathbb{R}^2 \setminus \Gamma \quad (8)$$

and, therefore,

$$\left[S_{\Gamma,k} \frac{\partial u}{\partial \nu} \right](\mathbf{x}) = u^{\text{inc}}(\mathbf{x}), \quad x \in \mathbb{R}^2 \setminus \Gamma. \quad (9)$$

This is a first kind integral equation. To improve the conditioning of this approach, we take the normal derivative of (9) as $\mathbf{x} \rightarrow \Gamma$, and add it to (8) multiplied by the factor $i\eta$. This results, for $\mathbf{x} \in \Gamma$, in the second kind integral equation

$$\left[\left(\frac{1}{2}I - S'_{\Gamma,k} + i\eta S_{\Gamma,k} \right) \frac{\partial u}{\partial \nu} \right](\mathbf{x}) = \frac{\partial u^{\text{inc}}}{\partial \nu}(\mathbf{x}) + i\eta u^{\text{inc}}(\mathbf{x}). \quad (10)$$

Once (10) is solved and $\frac{\partial u}{\partial \nu}$ is known, it is straightforward to see from (8) that the far field pattern is given by

$$u^\infty(\theta) = - \left[S_{\Gamma,k}^\infty \frac{\partial u}{\partial \nu} \right](\theta), \quad \theta \in U. \quad (11)$$

2.3 Numerical solution of the direct scattering problem

It remains to discuss the discretization and solution of (6) and (10). For this, we assume the boundary Γ is parametrized by $\gamma : [0, L] \rightarrow \mathbb{R}^2$, with $\gamma(0) = \gamma(L)$. We discretize the boundary using a Nyström method [1], with N equispaced points corresponding to $t_j = (j-1)L/N$ on the boundary for $j = 1, \dots, N$. We assign an unknown value $\varphi(t_j)$ or $\frac{\partial u}{\partial \nu}(t_j)$ at each such point and enforce the integral equation pointwise at the same points. If the domain Γ and the integrands in $S_{\Gamma,k}\varphi$, $D_{\Gamma,k}\varphi$ and $S'_{\Gamma,k}\varphi$ were smooth, the trapezoidal rule would yield a dense $N \times N$ matrix whose solution would be spectrally accurate (or superalgebraically convergent) [24, 25]. Because $S_{\Gamma,k}$ and the principal value for $D_{\Gamma,k}$ and $S'_{\Gamma,k}$ are logarithmically singular, however, we employ the hybrid Gauss-trapezoidal rule of order 16 due to Alpert [26]. Without entering into details, we simply note here that the hybrid Gauss-trapezoidal rule replaces the diagonal band (with bandwidth sixteen) of the matrix generated by the trapezoidal rule with special quadrature weights in order to achieve sixteenth order accuracy. Other high order quadrature methods could be used equally well [27, 28].

For small N , we use direct LU factorization to solve the discretized versions of (6) and (10). For large values of N , the $O(N^3)$ complexity makes the cost of naive LU factorization prohibitive. Given a well-conditioned formulation, one could use fast multipole-accelerated iterative solution methods such as GMRES. While this is asymptotically optimal, we are often interested in solving scattering problems in the same geometry with different right-hand sides. For this, recently developed fast direct solvers are more powerful. These methods make use of the fact that off-diagonal blocks of the system matrix representing (10) or (6) are low-rank to a user-specified precision and we refer the reader to the literature on hierarchical off-diagonal low-rank matrices (HODLR) [29, 30, 31], hierarchically semi-separable (HSS) or hierarchically block-separable (HBS) matrices [32, 33, 34, 35, 36, 37], and \mathcal{H} and \mathcal{H}^2 matrices [38, 39, 40, 41]. Here, we will employ the fast direct solver of

Ambikasaran and Darve [29], whose cost scales as $\mathcal{O}(N \log^2 N)$ for a fixed frequency, and which performs well even for problems that are many wavelengths in size.

Once the densities $\{\varphi(t_j)\}$ or $\{\frac{\partial u}{\partial \nu}(t_j)\}$ are known at the points $\{\gamma(t_j)\}$, we can calculate the far-field pattern at M points $\{\theta_\ell, \ell = 1, \dots, M\}$ on the unit circle using the trapezoidal rule for the far-field operators $S_{\Gamma,k}^\infty$ and $D_{\Gamma,k}^\infty$. Since the kernels of these operators are smooth (analytic), the trapezoidal rule yields spectral accuracy [25]. M is modest in our examples here, so we compute the far field directly, requiring $\mathcal{O}(NM)$ work. For larger-scale problems, fast algorithms are available to reduce the computational complexity [42, 43, 44].

3 The inverse scattering problem

With fast and accurate solvers available for the forward scattering problem, we turn to the development of an iterative method for the solution of the inverse problem (3)

$$F(\Gamma) = u^\infty.$$

That is, given the far-field pattern, we wish to determine the shape Γ of the scatterer itself. We will begin with a formulation of the problem for a single incident wave at a single frequency.

3.1 Inversion with a single incident direction

Let us assume for the moment that the incident plane wave is specified by the direction d at a single frequency k . As noted in the introduction, even the theoretical foundations for the inverse problem are rather complicated, with issues such as uniqueness and stability still active areas of research [1, 5]. Mathematically, the problem is that the operator F is a smoothing operator. More precisely [1], $F : C^1(\Gamma) \rightarrow L^2(U)$, where U is the unit circle is continuous, compact and Fréchet differentiable. Thus, inverting (3) is classically ill-posed. Physically, the problem is that subwavelength features give rise to evanescent waves which decay exponentially in space and are not detectable in finite precision from u^∞ (essentially, a version of the Heisenberg uncertainty principle).

Before turning to the question of regularization, we present an informal description of our iterative procedure—a Newton-like method to solve for the unknown Γ , based on the approximation

$$F(\Gamma_j + P_j) \approx F(\Gamma_j) + F'(\Gamma_j)P_j = u^\infty,$$

where Γ_j is the j th guess for Γ , $F'(\Gamma_j)$ denotes the Fréchet derivative of F , and P_j is the update. The $(j+1)$ st iterate is then given by

$$\Gamma_{j+1} = \Gamma_j + P_j. \tag{12}$$

Remark 3.1 *We note that the Fréchet derivative of a compact operator is itself compact, so that F' will inherit much of the ill-posedness of F .*

The approximation above leads to the linearized problem:

$$F'(\Gamma_j)P_j = u^\infty - F(\Gamma_j), \tag{13}$$

whose solution turns out to be fairly straightforward, due to a theorem of Kirsch [45].

Theorem 3.1 *Let Γ_j denote a closed boundary in \mathbb{R}^2 with u^{inc} a given incoming field, parametrized by $\gamma_j(t)$ in arclength for $t \in [0, L_j]$. Let u_j^{scat} denote the solution to the corresponding forward scattering problem, with Neumann data for the total field on Γ_j given by $\frac{\partial u_j}{\partial \nu}$ and far-field pattern $F(\Gamma_j)$. Let v denote the solution to the forward scattering problem with Dirichlet data*

$$v(t) = -\nu_j(t) \cdot P_j(t) \frac{\partial u_j}{\partial \nu}(t) \quad \text{on } \Gamma_j,$$

where $P_j(t)$ is some two-dimensional perturbation of the boundary and $\nu_j(t)$ denotes the normal vector to Γ_j . Finally, let v^∞ denote its far-field pattern. Then

$$F'(\Gamma_j)P_j = v^\infty. \quad (14)$$

Remark 3.2 *In order to make use of the preceding theorem, we need to first obtain the normal derivative $\partial u_j / \partial \nu$. This is accomplished by solving the integral equation (10) on Γ_j . Given this normal derivative data, we denote by \mathcal{B} the diagonal operator which corresponds to multiplication by $\partial u_j / \partial \nu(t)$. We then solve the Dirichlet problem for v using eq. (6) and apply the far field operator from (7), yielding*

$$\left(D_{\Gamma_j, k}^\infty - i\eta S_{\Gamma_j, k}^\infty \right) \left(\frac{1}{2}I + D_{\Gamma_j, k} - i\eta S_{\Gamma_j, k} \right)^{-1} \mathcal{B}(\nu_j \cdot P_j) = u^\infty - F(\Gamma_j). \quad (15)$$

Rather than letting P_j be an arbitrary perturbation of the curve Γ_j , however, we will assume that it lies in the normal direction:

$$P_j(t) = \nu_j(t)p_j(t),$$

where $p_j(t)$ is a scalar function. This avoids certain kinds of nonuniqueness which tangential motion of the boundary would permit, making the recovery even more ill-conditioned. Thus, eq. (15) is replaced by

$$\left[\left(D_{\Gamma_j, k}^\infty - i\eta S_{\Gamma_j, k}^\infty \right) \left(\frac{1}{2}I + D_{\Gamma_j, k} - i\eta S_{\Gamma_j, k} \right)^{-1} \mathcal{B} \right] p_j(t) = u^\infty - F(\Gamma_j). \quad (16)$$

Hereafter, we will refer to the operator on the left-hand side of eq. (16) acting on $p_j(t)$ as $F'(\Gamma_j)$. Several important features of the iteration remain to be discussed.

1. We must ensure that the curve Γ_{j+1} constructed via (12) is not self-intersecting. Therefore, we define

$$\Gamma_{j+1}^l = \Gamma_j + \rho \lambda^l P_j,$$

where ρ is a user-specified parameter, and $\lambda < 1$ provides additional damping of the Newton step if needed. We begin with $l = 0$ and accept the curve based on oversampling the curve Γ_{j+1}^l at a large number of points N_s . We check that the polygonal approximation of the curve is not self-intersecting. This is trivial to do using a naive $\mathcal{O}(N_s^2)$ algorithm. More sophisticated algorithms achieve a computational complexity of $\mathcal{O}(N_s \log N_s)$ [46, 47, 48]. If Γ_{j+1}^l fails to be simple, we increase l and repeat.

2. To overcome the ill-posedness of the problem, we will restrict p_j to be a band-limited curve:

$$p_j(t) = \sum_{m=-b/2}^{b/2-1} p_{j,m} e^{im2\pi t/L}. \quad (17)$$

We will return to the selection of the parameter b in section 4.1.

The integral equation (16) then takes the form of a “discrete-to-continuous” map, with b degrees of freedom which we can solve in a least squares sense. The fully discrete version of (16) is:

$$[A^\infty C^{-1} B O] \vec{p}_j = R$$

where A^∞ is an $M \times N$ discretization of $(D_{\Gamma_j,k}^\infty - i\eta S_{\Gamma_j,k}^\infty)$, C is an $N \times N$ discretization of $(\frac{1}{2}I + D_{\Gamma_j,k} - i\eta S_{\Gamma_j,k})$, B is a diagonal $N \times N$ matrix discretizing \mathcal{B} , O is an $N \times l$ matrix mapping the coefficients \vec{p}_j in (17) to equispaced samples of $p_j(t)$ on Γ_j and R is a discretization of the right-hand side $u^\infty - F(\Gamma_j)$ at M points. (We discretize the integral eq. operator C from (6) as described in section 2.) Thus, in the fully discrete version, we have $F' = A^\infty C^{-1} B O$, which is of dimension $M \times b$. We assume that M and b are sufficiently small that standard linear algebra tools for least squares problems can be applied, such as the QR factorization, so long as $M > b$.

3. It is more efficient to compute the entries of $(F')^T = O^T B^T C^{-T} (A^\infty)^T$ than F' itself, since we then need to apply C^{-T} to M distinct vectors, namely the columns of $(A^\infty)^T$. (We are assuming here that M is significantly smaller than N .) With the fast direct solver of [29], this requires $O(MN \log^2 N)$ work. The operator O^T can be applied using the fast Fourier transform at a net cost of $O(M(b+N) \log N)$ work.
4. After each iteration, we have a new boundary Γ_{j+1} sampled at N points: $\gamma_{j+1}(t_n) = \gamma_j(t_n) + \rho \lambda^m P_j(t_n) \nu_j(t_n)$, where m is determined by the acceptance criterion discussed above. To further improve the conditioning of the inverse problem, we use the algorithm of Beylkin and Rokhlin [18] to filter the curve Γ_{j+1} and return N points equispaced in arclength on this resampled curve. Without entering into details, we have implemented the algorithm of [18] to permit filtering of the curve beginning at frequency b , with a smooth roll-off until frequency $b + N_b$. On output, the algorithm returns N points equispaced in arclength with respect to the new (smooth) parameterization.
5. In our examples below, we choose Γ_0 to be the unit disk. Better initial guesses can be obtained by using a sampling method [12, 15, 14, 13, 11] which provides a good approximations to the convex hull of the unknown object.
6. In addition to the use of damping to ensure that the curve is simple (not self-intersecting), we need some stopping criteria for the Newton iteration. For this, we set a maximum number of Newton steps, a minimum norm for the solution to the linearized problem $|p_j(t)|$ and a residual tolerance ($\|F(\Gamma) - u^\infty\| < \epsilon$).

The choice of the parameter ρ in the damped Newton step can also be important [49, 50]. (Small values tend to require more iterations but can improve convergence.) In [51] Li and Bao suggest a frequency-dependent damping parameter. We have not explored this choice systematically in the present paper.

3.2 Inversion with multiple incident directions

Suppose now that we seek to solve the inverse problem when scattering data is available from several angles of incidence. Let L denote the number of incident plane waves:

$$u_m^{\text{inc}}(\mathbf{x}) = e^{ik\mathbf{x} \cdot \mathbf{d}_l}$$

with directions \mathbf{d}_l for $l = 1, \dots, L$. To solve this problem, eq. (13) is replaced at each iteration by the system of equations:

$$\begin{bmatrix} F'_1(\Gamma_j) \\ F'_2(\Gamma_j) \\ \vdots \\ F'_L(\Gamma_j) \end{bmatrix} P_j = \begin{bmatrix} u^\infty - F_1(\Gamma_j) \\ u^\infty - F_2(\Gamma_j) \\ \vdots \\ u^\infty - F_L(\Gamma_j) \end{bmatrix} \quad (18)$$

where F_l is the far-field operator on Γ_j for data generated by the incident plane wave $u_l^{\text{inc}}(\mathbf{x})$ and F'_l is its Fréchet derivative.

The discretization of each of the operators F_l and F'_l is carried out as in the previous section. Note that, since the unknown in the fully discrete version of (18) is still \vec{p}_j , we can only improve the conditioning of the least squares problem when compared to the setting with a single angle of incidence. This makes physical sense; illuminating the unknown obstacle from more directions should certainly make the recovery problem easier.

4 Multiple frequency measurements and recursive linearization

Since the number of nontrivial measurements that can be made in the far field is proportional to the size of the object in wavelengths, it is reasonable to expect that greater resolution should be obtained as the frequency increases. There are fundamental difficulties, however, with using Newton's method (or one of its variants) for inverse scattering at a single frequency k . Mainly, when k is large, the initial guess for the boundary shape Γ must be close to the correct solution in order for the iteration not to diverge or be trapped in a spurious local minimum. Moreover, only the "illuminated" portion of the boundary can be recovered with fidelity, as discussed in [52]. When k is small, however, despite the fact that the inverse scattering problem is ill-posed, if one only seeks to recover a small number of parameters (say the centroid and area of the scatterer), a few Newton iterations are sufficient for convergence *without* a good initial guess.

This interplay between easy recovery at low frequencies of a blurry reconstruction and the need for a good initial guess at high frequency to achieve higher fidelity reconstruction led Chen [19] to introduce the *recursive linearization algorithm* (RLA). The essential idea is that given the (blurry but converged) solution to the inverse scattering problem at frequency k , one step of Newton's method is sufficient to get the converged solution for frequency $k + \delta k$, for sufficiently small δk . That is the sense in which the problem has been linearized. It has been used previously by Sini and Thanh [20] and Borges [52] for the inverse obstacle problem for a single angle of incidence with an unknown star-shaped object. The procedure is initiated at a sufficiently small frequency k so that Newton's method converges without a good initial guess. We refer the reader to [19] for a more detailed explanation.

When a finite number of frequency measurements are available, $k_1 < k_2 < \dots < k_J$, a modification of RLA is to begin at the lowest frequency k_1 and to solve the inverse scattering problem to obtain a guess which we will denote by $\Gamma^{(k_1)}$. $\Gamma^{(k_1)}$ can then be used as the initial guess for a new Newton iteration at frequency k_2 , with the recursion continuing until the maximum frequency k_J has been reached. A formal theory, of course, might require tight control on the spacing in frequency $\delta k = k_{j+1} - k_j$, and we use the RLA framework here simply as a sensible guideline, as in [52, 20].

In summary, for the multi-frequency, multi-direction problem, we assume we are given measurements of the far-field pattern at M angular points θ_l , generated by the scattering of $J \cdot L$ incident plane waves $u_{j,l}^{\text{inc}}(x) = e^{ik_j \mathbf{x} \cdot \mathbf{d}_l}$ for $l = 1, 2, \dots, L$ and $j = 1, 2, \dots, J$, where $k_1 < k_2 < \dots < k_J$. The goal, as always, is to reconstruct the unknown object Ω with boundary Γ .

4.1 Setting the bandlimit

In order for the inverse problem to be well-conditioned at each frequency, it is important to choose the parameter b in (17) correctly. The value of b determines how complicated a curve we are able to reconstruct since it controls the complexity of the perturbation $P_j(t)$. Clearly, its value should be approximately proportional to k in order to achieve the best possible resolution. Smaller values would lead to stable but excessively pessimistic reconstructions while larger values would permit subwavelength instabilities to develop.

5 Numerical experiments

In this section, we illustrate the performance of our inverse obstacle scattering algorithm. Before turning to specific examples, a few general remarks are in order. First, with a single incident wave, we should not expect to obtain a good reconstruction of the poorly illuminated “backside” of the boundary. (This effect is more pronounced at higher frequencies [52, 20].) With multiple directions of incidence, however, it should be possible to reconstruct the entire object with much greater fidelity. Second, because we are carrying out our reconstruction over the space of band-limited closed curves, geometric singularities and regions of high curvature will inevitably be filtered (with the extent of filtering a decreasing function of frequency.)

For each object, we construct simulated measurement data in the far field pattern by solving the direct scattering problem, as discussed in Section 2. We compute the solution to (10) or (6) with at least ten digits of accuracy to generate far field data $u_{k,\mathbf{d}}^\infty$ and then introduce Gaussian noise in the data. Here k denotes the frequency and \mathbf{d} the direction of incidence. We set

$$v_\infty^{k,\mathbf{d}} = u_{k,\mathbf{d}}^\infty + \delta \frac{\|u_{k,\mathbf{d}}^\infty\|}{\|\epsilon_1 + i\epsilon_2\|} (\epsilon_1 + i\epsilon_2),$$

where ϵ_1 and ϵ_2 are normally distributed variables with mean zero and variance one. As in [53], we also make sure to use a different number of quadrature points in the discretization of the direct problem and in the integral equations used in solving the inverse problem.

In our examples, we use $\delta = 0.05$, and let $\mathbf{d}_l = 2\pi l/L$ (for $l = 1, \dots, L$) for wavenumbers $k_j = k_0 + j\Delta k$ with $j = 1, \dots, J$. The far field pattern is obtained at the angles $\theta_\ell = (2\ell - 1)\pi/M$, for $\ell = 1, \dots, M$. At each wavenumber k , the number of quadrature points used in solving the direct scattering problem is $N = \lceil 100k|\Gamma| \rceil$, where $|\Gamma|$ is the perimeter of the object. The number

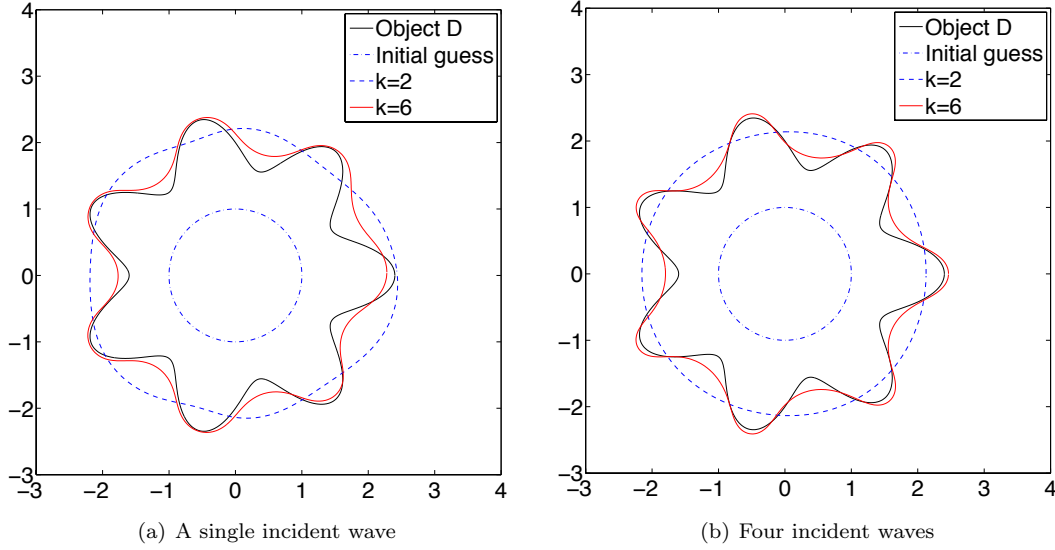


Figure 1: Reconstruction using recursive linearization with Newton's method for the object in Example 1 for $L = 1$ (a) and for $L = 4$ (b).

of collocation points used in solving the inverse problem is denoted by N_1 . The specific values for M , L , J , k_0 , Δk and N_1 are described for each numerical experiment below.

Example 5.1 *A star-shaped object with 7 oscillations*

In our first example, we consider a star-shaped object with parameterization $\gamma : [0, 2\pi] \rightarrow \mathbb{R}^2$ given by

$$\gamma(t) = (2 + 0.2 \cos(7t)) (\cos(t), \sin(t)). \quad (19)$$

The initial wavenumber is $k_0 = 0.5$, $\Delta k = 0.5$, and $J = 11$. We let $M = 32$ and use the damping parameter $\rho = 0.1$ for wavenumbers up to $k = 5$ and $\rho = 0.1/k$ for higher wavenumbers. Within Newton's method, the stopping criterion used for the nonlinear residual is $\epsilon = \|F(\Gamma) - u^\infty\| < 10^{-4}$. We used $N_1 = \lceil 10k|\Gamma_j| \rceil$ quadrature points in solving the integral equations within the Newton step. In Fig. 1(a), we plot the reconstruction using a single direction of incidence, $L = 1$, and use the bandlimit $b = \lceil k \rceil$ at each wavenumber, while in Fig. 1(b) we plot the reconstruction for $L = 4$ and use the bandlimit $b = 2\lceil k \rceil + 1$. In both cases, the filter in the curve resampling algorithm uses a smooth roll-off from b to $b + 50$. In both cases, we show the solutions obtained for $k = 2$ and $k = 6$. The reason we can choose a larger value for b when using multiple angles of incidence is that the system matrix (18) remains well-conditioned, as noted in section ??.

To illustrate the advantage of solving the forward scattering problem using the integral equation (6) by applying the HODLR algorithm, we compare the run-time of HODLR and direct factorization for problems with increasing wavenumber k and number of discretization points, using the star-shaped object with 7 oscillations as the geometry. The error is computed by taking as boundary data the field induced by a singular point source at the origin, which lies in the interior of the scatterer and testing the computed exterior solution at the target point $(10, 8)$.

Table 1: Running time for direct scattering problem

k	N	Direct solver		HODLR	
		Time(s)	Error	Time(s)	Error
1	360	0.17	7.711837e-13	0.72	7.715468e-13
2	720	0.57	1.764748e-12	1.64	1.766015e-12
4	1440	2.08	3.097516e-12	3.80	3.094913e-12
8	2880	7.19	1.988648e-12	7.91	2.120391e-12
16	5760	33.48	2.298391e-11	17.20	2.303258e-11
32	11520	314.83	1.957544e-11	37.91	1.939017e-11
64	23040	—	—	95.44	3.924397e-11
128	46080	—	—	278.49	9.649962e-11

Note that the direct solver is faster than the HODLR for small problems, but that it scales much better with N . The run-times for direct factorization are omitted for the largest problems, since prohibitive amounts of memory would be needed.

Example 5.2 *An aircraft-like object*

We next consider a more complicated (and not star-shaped) object, shown in Figs. 2(a)-2(d). Our initial guess is the circle of radius 1 centered at the origin. We used an initial wavenumber of $k_0 = 0.5$, with $\Delta k = 0.5$, and $J = 60$, and let the number of far-field measurements be $M = 128$. Within Newton's method, the stopping criterion used for the nonlinear residual is $\epsilon = \|F(\Gamma) - u^\infty\| < 10^{-3}$. We used $N_1 = \lceil 20k|\Gamma_j| \rceil$ quadrature points in solving the integral equations within the Newton step and let the damping parameter $\rho = 1$.

In order to show the improvement of the reconstruction using an increasing number of incident plane waves, we present the final reconstructions for the cases $L = 1, 2, 3, 4$ with $b = 2\lceil k \rceil + 1$ (Figs. 2(a) - 2(d)).

Finally, we present a reconstruction using six directions of incidence and the bandlimit $b = 2\lceil k \rceil + 1$, with a smooth roll-off in the curve resampling from b to $b + 130$. All other parameters are chosen as before. In Fig. 3(a), we plot the solution obtained with our scheme for varying maximum frequencies. In Figs. 3(b)–3(d), we present zoomed in details of the reconstruction in certain high-curvature regions of the object.

Example 5.3 *Reconstruction of an elongated object*

In our final example, we reconstruct an object with a submarine-like shape. Our initial guess is the circle of radius 1 centered at the origin. The initial wavenumber is $k_0 = 0.1$, with $\Delta k = 0.4$, and $J = 57$. We let the number of far field measurements be $M = 128$ and assumed six directions of incidence ($L = 6$). We choose the damping parameter $\rho = 1$. We use the bandlimit $b = 2\lceil k \rceil + 1$ at each wavenumber, with a smooth roll-off in the curve resampling filter from b to $b + 50$. Within Newton's method, the stopping criterion used for the nonlinear residual is $\epsilon = \|F(\Gamma) - u^\infty\| < 10^{-3}$. We used $N_1 = \lceil 20k|\Gamma_j| \rceil$ quadrature points in solving the integral equations within the Newton step. In Fig. 4(a), we plot the solution obtained for various maximal frequencies. Figs. 4(b)–4(d) show details of the reconstruction in certain high curvature regions of the object.

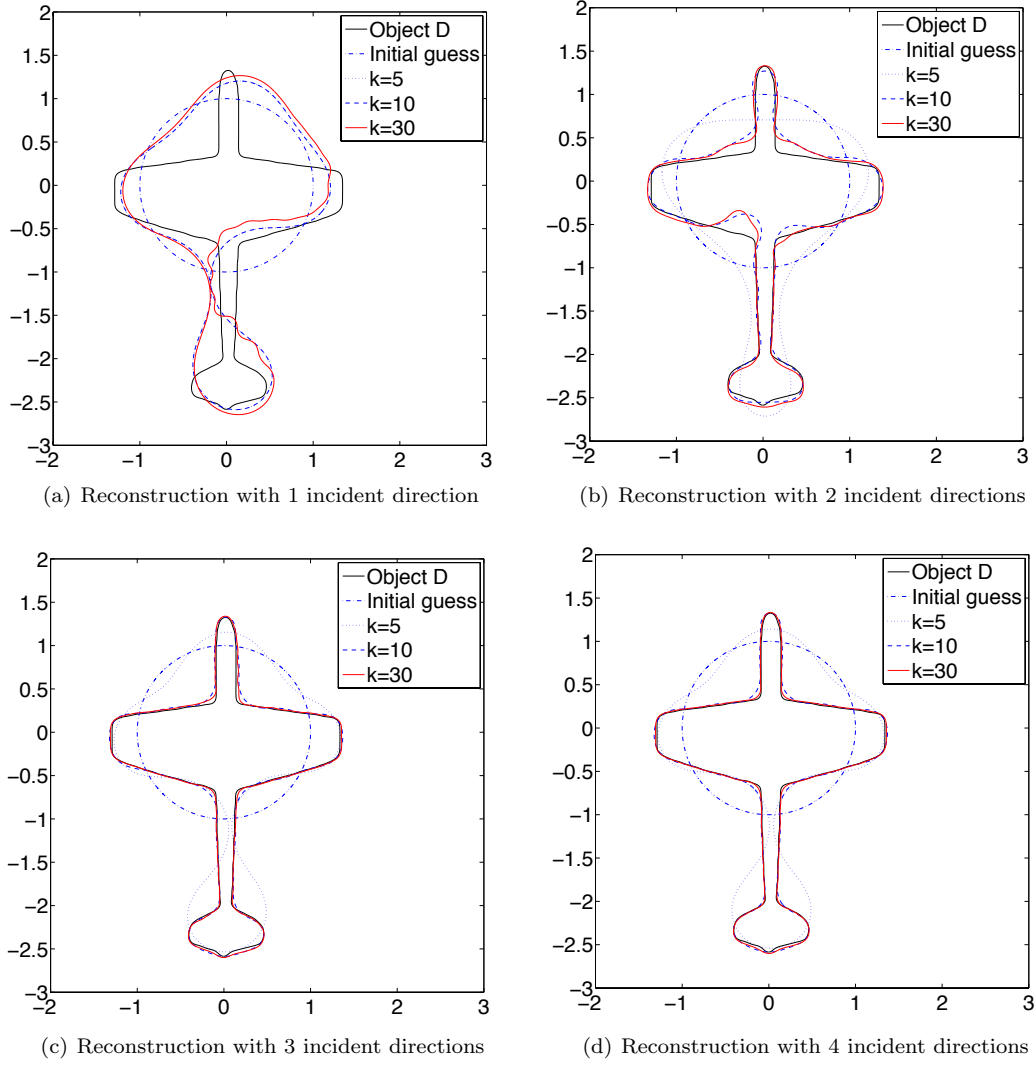


Figure 2: Reconstruction of the aircraft-like object using Newton's method with an increasing number of incident directions.

The number of Newton iterations at each frequency to recover the aircraft-like and submarine-like objects are shown in Fig. 5.

Note that a large number of damped steps are required at the lowest frequency, when the initial guess is very far from the correct shape, but that the number decreases significantly after that.

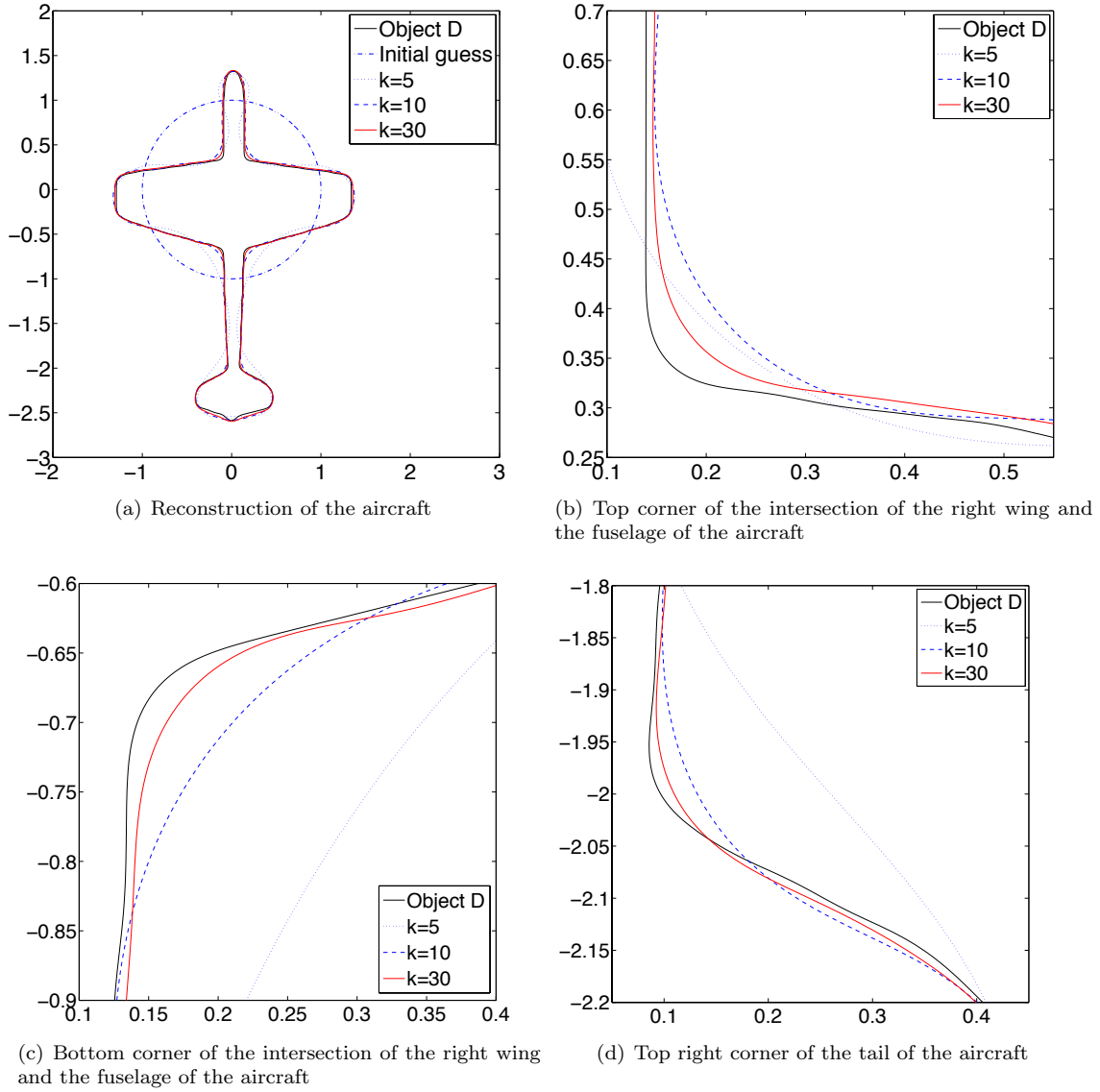


Figure 3: Reconstruction using recursive linearization with Newton's method to reconstruct the aircraft-like object of Example 2.

6 Conclusion

We have presented a technique for reconstructing the shape of two-dimensional sound-soft obstacles, given the far-field pattern, using multiple angles of incidence and multiple frequencies. While the problem is both ill-posed and nonlinear, a combination of techniques makes it tractable. First, we reduce the number of degrees of freedom to be determined based on physical considerations (the

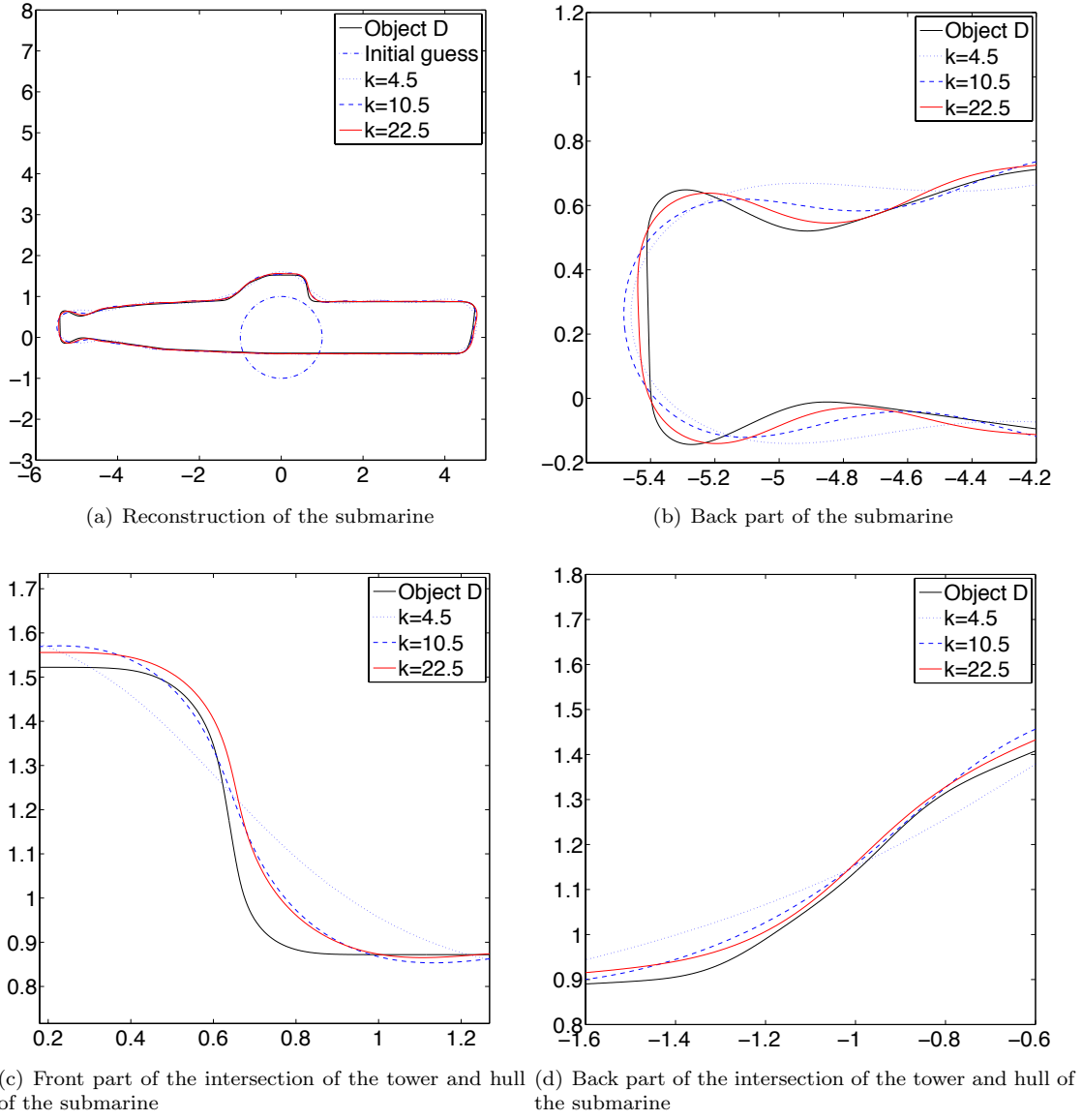


Figure 4: Reconstruction using recursive linearization with Newton's method to reconstruct the submarine-like object.

approximate dimensions of the object in wavelengths). We do not make use of Tikhonov regularization or other generic regularization schemes. Second, when multiple frequency data is available, we make use of recursive linearization [19]. In our experiments, Newton's method with damping has trouble converging at the lowest frequency, when the initial guess is far from the desired minimum. Subsequently, recursive linearization enables rapid convergence, consistent with the analysis

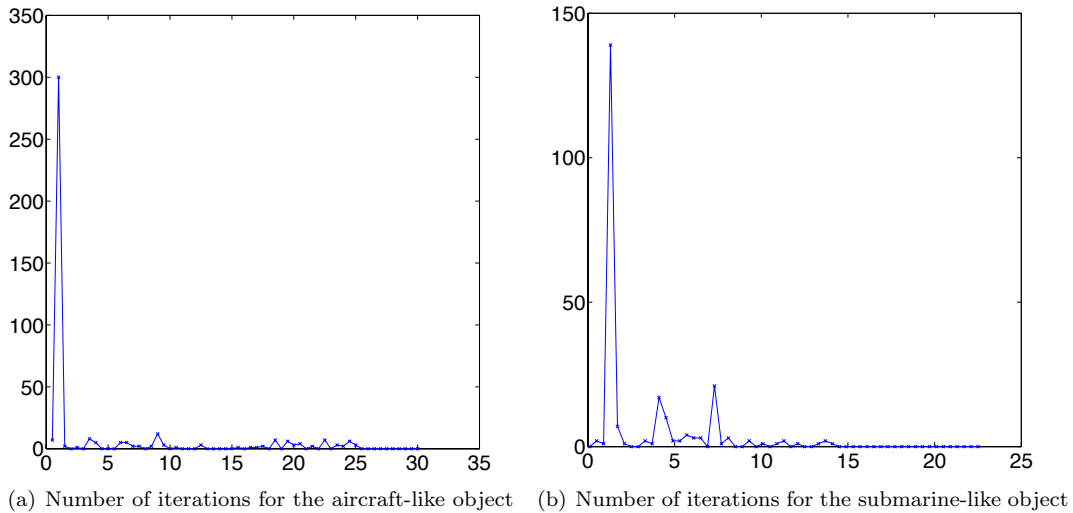


Figure 5: Number of iterations for the Newton's method at each wavenumber k .

of Sini and Thành [20]. In our method, we also make use of the fact that the conditioning of the reconstruction problem is improved by using multiple angles of incidence. Finally, we employ high-order accurate discretizations and the HODLR fast solver to accelerate the solution of the necessary forward scattering problems, so that all our experiments are easily carried out using modest computational resources. Unlike many algorithms for the inverse obstacle scattering problem, we make no assumption about the parametrization of the geometry, such as being star-shaped. In our present formulation, however, we do assume that the obstacle is a single, simply-connected region in the plane.

The method is easily extended to the case of sound-hard obstacles or impedance boundary conditions. Moreover, most aspects have straightforward three-dimensional analogs: recursive linearization, high-order discretization and fast, forward scattering solvers (although the latter two are still areas of active research). One aspect that is not so straightforward concerns the development of a simple and robust parametrization of surfaces which permits “physical regularization” - systematically reducing the number of degrees of freedom to be solved for in each linearized problem by enforcing some kind of band-limit on the perturbation. We are currently considering a variety of approaches for this and progress will be reported at a later date.

Two issues we have not addressed here are inverse obstacle scattering when only partial aperture data is available and when only the magnitude of the far field is measured, rather than magnitude and phase. These are of significant practical importance and also active areas of research.

Acknowledgments

The work reported was supported by the Air Force Office of Scientific Research under grant number FXXXXX-XX- X-XXXX. The authors also gratefully acknowledge the valuable comments and suggestions of Michael O’Neil and Sivaram Ambikasaran.

References

- [1] D. Colton and R. Kress, *Inverse Acoustic and Electromagnetic Scattering Theory*. Springer, 2nd ed., 1998.
- [2] V. Isakov, *Inverse Problems for Partial Differential Equations*. No. 127 in Applied Mathematical Sciences, Springer, 1998.
- [3] A. Kirsch, *An Introduction to the Mathematical Theory of Inverse Problems*. Applied Mathematical Sciences, Springer, 2011.
- [4] P. Kuchment, *The Radon Transform and Medical Imaging*. CBMS-NSF Regional Conference Series in Applied Mathematics, Society for Industrial and Applied Mathematics, 2014.
- [5] R. Kress, “Uniqueness and numerical methods in inverse obstacle scattering,” *Journal of Physics: Conference Series*, vol. 73, no. 1, p. 012003, 2007.
- [6] T. Hohage, “Logarithmic convergence rates of the iteratively regularized Gauss - Newton method for an inverse potential and an inverse scattering problem,” *Inverse Problems*, vol. 13, no. 5, pp. 1279–1299, 1997.
- [7] R. Kress, “Newton’s method for inverse obstacle scattering meets the method of least squares,” *Inverse Problems*, vol. 19, no. 6, pp. S91–S104, 2003.
- [8] A. Kirsch and R. Kress, “An optimization method in inverse acoustic scattering,” *Boundary Elements IX*, vol. 3, pp. 3–18, 1987.
- [9] R. Potthast, “A fast new method to solve inverse scattering problems,” *Inverse Problems*, vol. 12, no. 5, pp. 731–742, 1996.
- [10] R. Potthast, “A point source method for inverse acoustic and electromagnetic obstacle scattering problems,” *IMA Journal of Applied Mathematics*, vol. 61, no. 2, pp. 119–140, 1998.
- [11] R. Potthast, *Point Sources and Multipoles in Inverse Scattering Theory*. Chapman & Hall/CRC Research Notes in Mathematics, Taylor & Francis Group, 2001.
- [12] D. Colton and A. Kirsch, “A simple method for solving inverse scattering problems in the resonance region,” *Inverse Problems*, vol. 12, no. 4, pp. 383–393, 1996.
- [13] R. Potthast, “Stability estimates and reconstructions in inverse acoustic scattering using singular sources,” *Journal of Computational and Applied Mathematics*, vol. 114, no. 2, pp. 247–274, 2000.
- [14] A. Kirsch, “Characterization of the shape of a scattering obstacle using the spectral data of the far field operator,” *Inverse Problems*, vol. 14, no. 6, pp. 1489–1512, 1998.
- [15] M. Ikehata, “Reconstruction of an obstacle from the scattering amplitude at a fixed frequency,” *Inverse Problems*, vol. 14, no. 4, pp. 949–954, 1998.
- [16] F. Cakoni and D. Colton, *Qualitative Methods in Inverse Scattering Theory: An Introduction*. Interaction of Mechanics and Mathematics, Springer, 2006.

- [17] J. Kaipio and E. Somersalo, *Statistical and Computational Inverse Problems*. Applied Mathematical Sciences, Springer, 2010.
- [18] D. Beylkin and V. Rokhlin, “Fitting a bandlimited curve to points in a plane,” Tech. Rep. YALEU/DCS/TR-1480, Department of Computer Science, Yale University, New Haven, CT, July 2013.
- [19] Y. Chen, “Inverse scattering via Heisenberg’s uncertainty principle,” *Inverse Problems*, vol. 13, no. 2, pp. 253–282, 1997.
- [20] M. Sini and N. G. Thành, “Inverse acoustic obstacle scattering problems using multifrequency measurements,” *Inverse Problems and Imaging*, vol. 6, no. 4, pp. 749–773, December 2012.
- [21] G. Bao and F. Triki, “Error Estimates for the Recursive Linearization of Inverse Medium Problems,” *Journal of Computational Mathematics*, vol. 28, pp. 725–744, July 2010.
- [22] J.-C. Nédélec, *Acoustic and Electromagnetic Equations*. Springer, 2001.
- [23] R. Kress, *Minimizing the condition number of boundary integral operators in acoustic and electromagnetic scattering*. NAM-Bericht: Institut für Numerische und Angewandte Mathematik, Inst. für Numerische und Angewandte Mathematik, Univ., 1983.
- [24] P. J. Davis and P. Rabinowitz, *Methods of Numerical Integration*. Academic Press, 1984.
- [25] R. Kress, *Linear Integral Equations*. No. 82 in Applied Mathematical Sciences, Springer New York, 1999.
- [26] B. K. Alpert, “Hybrid Gauss-Trapezoidal Quadrature Rules,” *SIAM Journal on Scientific Computing*, vol. 20, pp. 1551–1584, 1999.
- [27] J. Helsing and R. Ojala, “Corner singularities for elliptic problems: integral equations, graded meshes, and compressed inverse preconditioning,” *J. Comput. Phys.*, vol. 227, pp. 8820–8840, 2008.
- [28] A. Klöckner, A. Barnett, L. Greengard, and M. O’Neil, “Quadrature by expansion: A new method for the evaluation of layer potentials,” *J. Comput. Physics*, vol. 252, pp. 332–349, 2013.
- [29] S. Ambikasaran and E. Darve, “An $O(N \log N)$ fast direct solver for partial hierarchically semi-separable matrices — with application to radial basis function interpolation,” *J. Sci. Comput.*, no. 3, pp. 477–501, 2013.
- [30] A. Aminfar, S. Ambikasaran, and E. Darve, “A fast block low-rank dense solver with applications to finite-element matrices,” *arXiv preprint arXiv:1403.5337 [cs-NA]*, 2014.
- [31] W. Y. Kong, J. Bremer, and V. Rokhlin, “An adaptive fast direct solver for boundary integral equations in two dimensions,” *Applied and Computational Harmonic Analysis*, vol. 31, no. 3, pp. 346–369, 2011.
- [32] L. Greengard, D. Gueyffier, P.-G. Martinsson, and V. Rokhlin, “Fast direct solvers for integral equations in complex three-dimensional domains,” *Acta Numerica*, vol. 18, no. 1, pp. 243–275, 2009.

- [33] S. Chandrasekaran, P. Dewilde, M. Gu, W. Lyons, and T. Pals, “A fast solver for HSS representations via sparse matrices,” *SIAM Journal on Matrix Analysis and Applications*, vol. 29, no. 1, pp. 67–81, 2006.
- [34] S. Chandrasekaran, M. Gu, and T. Pals, “A fast ULV decomposition solver for hierarchically semiseparable representations,” *SIAM Journal on Matrix Analysis and Applications*, vol. 28, no. 3, pp. 603–622, 2006.
- [35] K. L. Ho and L. Greengard, “A fast direct solver for structured linear systems by recursive skeletonization,” *SIAM Journal on Scientific Computing*, vol. 34, no. 5, pp. 2507–2532, 2012.
- [36] P.-G. Martinsson, “A fast direct solver for a class of elliptic partial differential equations,” *Journal of Scientific Computing*, vol. 38, no. 3, pp. 316–330, 2009.
- [37] P.-G. Martinsson and V. Rokhlin, “A fast direct solver for boundary integral equations in two dimensions,” *Journal of Computational Physics*, vol. 205, no. 1, pp. 1–23, 2005.
- [38] M. Bebendorf, “Hierarchical LU decomposition-based preconditioners for BEM,” *Computing*, vol. 74, no. 3, pp. 225–247, 2005.
- [39] S. Börm, L. Grasedyck, and W. Hackbusch, “Hierarchical matrices,” *Lecture notes*, vol. 21, 2003.
- [40] S. Börm, L. Grasedyck, and W. Hackbusch, “Introduction to hierarchical matrices with applications,” *Engineering Analysis with Boundary Elements*, vol. 27, no. 5, pp. 405–422, 2003.
- [41] W. Hackbusch, L. Grasedyck, and S. Börm, *An introduction to hierarchical matrices*. Max-Planck-Inst. für Mathematik in den Naturwiss., 2001.
- [42] E. Candes, L. Demanet, and L. Ying, “Fast computation of fourier integral operators,” *SIAM J. Sci. Comput.*, vol. 29, pp. 2464–2493, 2007.
- [43] I. Sammis and J. Strain, “A geometric nonuniform fast fourier transform,” *J. Comput. Phys.*, vol. 228, pp. 7086–7108, 2009.
- [44] M. O’Neil, F. Woolfe, and V. Rokhlin, “An algorithm for the rapid evaluation of special function transforms,” *Appl. Comput. Harmon. Anal.*, vol. 28, pp. 203–226, 2010.
- [45] A. Kirsch, “The domain derivative and two applications in inverse scattering theory,” *Inverse Problems*, vol. 9, no. 1, pp. 81–96, 1993.
- [46] J. L. Bentley and T. A. Ottmann, “Algorithms for reporting and counting geometric intersections,” *IEEE Trans. Comput.*, vol. 28, pp. 643–647, Sept. 1979.
- [47] F. P. Preparata and M. I. Shamos, *Computational Geometry: An Introduction*. New York, NY, USA: Springer-Verlag New York, Inc., 1985.
- [48] M. I. Shamos and D. Hoey, “Geometric intersection problems,” in *Proceedings of the 17th Annual Symposium on Foundations of Computer Science*, SFCS ’76, (Washington, DC, USA), pp. 208–215, IEEE Computer Society, 1976.

- [49] A. R. Conn, N. I. M. Gould, and P. L. Toint, *Trust-region methods*. MPS/SIAM Series on Optimization, Philadelphia, PA: Society for Industrial and Applied Mathematics (SIAM), 2000.
- [50] J. E. Dennis, Jr. and R. B. Schnabel, *Numerical methods for unconstrained optimization and nonlinear equations*, vol. 16 of *Classics in Applied Mathematics*. Philadelphia, PA: Society for Industrial and Applied Mathematics (SIAM), 1996. Corrected reprint of the 1983 original.
- [51] G. Bao and P. J. Li, “Shape Reconstruction of Inverse Medium Scattering for the Helmholtz Equation,” in *Computational Methods for Applied Inverse Problems* (Y. Bai, G. Bao, and J. J. C. et al., eds.), pp. 283–306, Berlin, Boston: De Gruyter, 2012.
- [52] C. Borges, *A multifrequency method for the solution of the acoustic inverse scattering problem*. Ph.D. dissertation, Worcester Polytechnic Institute, 2012. 130 p.
- [53] O. Ivanyshyn and T. Johansson, “Nonlinear integral equation methods for the reconstruction of an acoustically sound-soft obstacle,” *Journal of Integral Equations and Applications*, vol. 19, no. 3, pp. 289–308, 2007.